# The path for innovative severe accident neutronics studies in ZPRs – Analysis of SNEAK-12B experiments for core disruption in LMFBRs

Marat Margulis [a,b], Patrick Blaise [b], Fabrizio Gabrielli [c], Adrien Gruel [b], Frederic Mellier [b], Erez Gilad [a,*]

[a] The Unit of Nuclear Engineering, Ben-Gurion University of the Negev, Beer-Sheva 84105, Israel
[b] DEN/CAD/DER/SPEx/LPE, CEA Cadarache, Saint-Paul-lès-Durance 13108, France
[c] Karlsruhe Institute of Technology (KIT), Hermann-von-Helmholtz-Platz 1, Eggenstein-Leopoldshafen 76344, Germany

A B S T R A C T

The present work details information (core geometry, material balance, and criticality measurements and calculations) regarding a new benchmark to be introduced to the international community, for dealing with neutronic code validation in the frame of the analysis of severe accidents in fast reactors leading to core degradation and material relocation. This specific benchmark is based on analysis of selected experiments performed at the Schnelle Null-Energie-Anordnung Karlsruhe (SNEAK). Unlike the previously analyzed SNEAK-12A core, which was loaded with enriched metallic uranium fuel, the core analyzed in this study, the SNEAK-12B core, was loaded with plutonium fuel to better represent future fast systems, and the experiments that were considered include fuel relocation and redistribution of structural material. In this paper, the experimental results are analyzed by computational tools such as MCNPX2.7 and Serpent-2.1.29 Monte Carlo codes, and the ERANOS 2.4 system code for deterministic calculations, all based on JEFF-3.1.1 nuclear data libraries. The paper provides a complete and detailed specification for the benchmark problem. Preliminary results of available experimental results ($k_{eff}$ and axial distribution of reaction rates) are given and additional quantities are presented (such as axial flux distribution). The benchmark offers an excellent opportunity to validate calculation schemes for strongly heterogeneous configurations, in particular the preparation of homogenized self-shielded neutron cross-sections for deterministic core calculations, as well as leakage treatment in locally voided zones. The analyses of SNEAK experiments, presented in this paper, provide grounds for the design of innovative experimental capabilities in severe accident modeling in Zero Power Reactors (ZPR), such as the Zero-power Experimental PHYsics Reactor (ZEPHYR) project led independently by the Commissariat à l'Énergie Atomique et aux Énergies Alternatives (CEA). This paper is completed by a comprehensive nuclear data sensitivity and uncertainty analysis of the reactivity coefficients and $k_{eff}$ in a companion paper.

© 2018 Elsevier Ltd. All rights reserved.

## 1. Introduction

The reactivity effects of material rearrangement, simulating conditions in postulated Liquid Metal-cooled Fast Breeder Reactors (LMFBRs) are currently studied in the framework of a joint work between the Commissariat à l'Énergie Atomique et aux Énergies Alternatives (CEA) Cadarache Research Center and Ben-Gurion University of the Negev for future Zero Power Reactor (ZPRs) experimental programs (Blaise et al., 2016). In order to design an experimental program which is highly representative of real LMFBR, it is necessary to revisit past experiments of severe core accidents (SCA), such as the SNEAK-12 program (Helm et al., 1984; Helm and Henneges, 1985; Henneges, 1988).

The first Schnelle Null-Energie-Anordnung Karlsruhe (SNEAK)-12A program (Helm et al., 1984) was aimed at study effects of sodium voiding and fuel relocation. The SNEAK-12A core had a single zone core fueled with metallic uranium plates. The results of those experiments were re-evaluated with advanced tools (Margulis et al., 2017a), such as Monte Carlo N-Particle (MCNP) (X-5 Monte Carlo Team, 2003), TRIPOLI (Brun et al., 2015), Serpent (Leppanen et al., 2015) and ERANOS (Ruggieri et al., 1973). The results showed an excellent agreement between the different codes and the measured reactivity changes between the different configurations. Furthermore, additional investigation of the experimental data was made, which included sensitivity and propagated uncertainties associated with the cross section data of isotopes with high importance to the behavior of the system (Margulis et al., 2017b). The analysis revealed a high level of uncertainties

**Acronyms**

| | | | |
|---|---|---|---|
| CDA | Core Disruptive Accident | SNEAK-12 | Schnelle-Null-Energie-Anordnung Karlsruhe 12 |
| CEA | Commissariat à l'Énergie Atomique et aux Énergies Alternatives | SS | Stainless Steel |
| | | TMI | Three Mile Island |
| ECCO | European Cell COde | ZEPHYR | ZEro power PHYsics Reactor |
| FBR | Fast Breeder Reactor | ZPR | Zero Power Reactor |
| LMFBR | Liquid Metal-cooled Fast Breeder Reactor | | |
| SCA | Severe Core Accident | | |

associated with the nuclear data that should be taken into account when designing new experiments.

However, in terms of representativity, the fuel loaded in the SNEAK-12A is different from the fuel that would be utilized in future Fast Breeder Reactors (FBRs). Therefore, it is of interest to compile a benchmark for code validation for plutonium-fuel-based reactors. The SNEAK-12B (Helm and Henneges, 1985; Henneges, 1988) experiments were performed using fuel loading of $PuO_2/UO_2$ rods in the central test zone, thus increasing the representativity of the experiment with regard to a Mixed OXides (MOX) fueled power reactor. In this paper, full summary and re-evaluation of the SNEAK-12B experimental results are presented.

The experiments in the SNEAK-12B program included axial movement of fuel towards the core center (slump-in) and away from the core center (slump-out), as well as axial movement of fuel from the top of the core to its bottom (slump-through). Additional experiments included steel blockage of streaming channels and radial material redistribution. Most of the data for the core layout was available in the SNEDAX database (Helm, 1996). However, the experimental values are not included in the SNEDAX database except for the clear core criticality measurements. The rest of the information regarding the experimental results was collected and compiled from personal notes of the team that operated the reactor. Therefore, one of the goals of this paper is to create a compre-

hensive summary of all the data regarding SNEAK-12B program (material balance, geometry, core layout, and experimental data).

The more realistic fuel composition used in the SNEAK-12B program makes this benchmark very attractive for the nuclear community. This benchmark is accompanied by advanced computer codes calculations and additional critical experiments, which further elaborate and expand the knowledge already obtained from the SNEAK-12A program (Margulis et al., 2017a,b). These studies may be used to narrow down the knowledge gap related to core physics phenomena (Devictor, 2013), such as the experimental validation of recriticality scenarios in fast reactors or monitoring and early identification of SCA (Margulis et al., 2018). Furthermore, the second benchmark from the SNEAK-12 program contributes additional information to the initiated experimental program at CEA Cadarache, aiming to study neutronic behavior of fast reactor SCA that would be implemented in the Zero power Experimental PHYsics Reactor (ZEPHYR) (Blaise et al., 2016).

## 2. SNEAK-12B – benchmark specification

This section provides a short overview of the SNEAK-12B core geometry, loaded with plutonium-oxide/uranium-oxide fuel rods as described in Section 2.1. The fuel selection was made according to the desire to examine the behavior of plutonium fuel under SCA
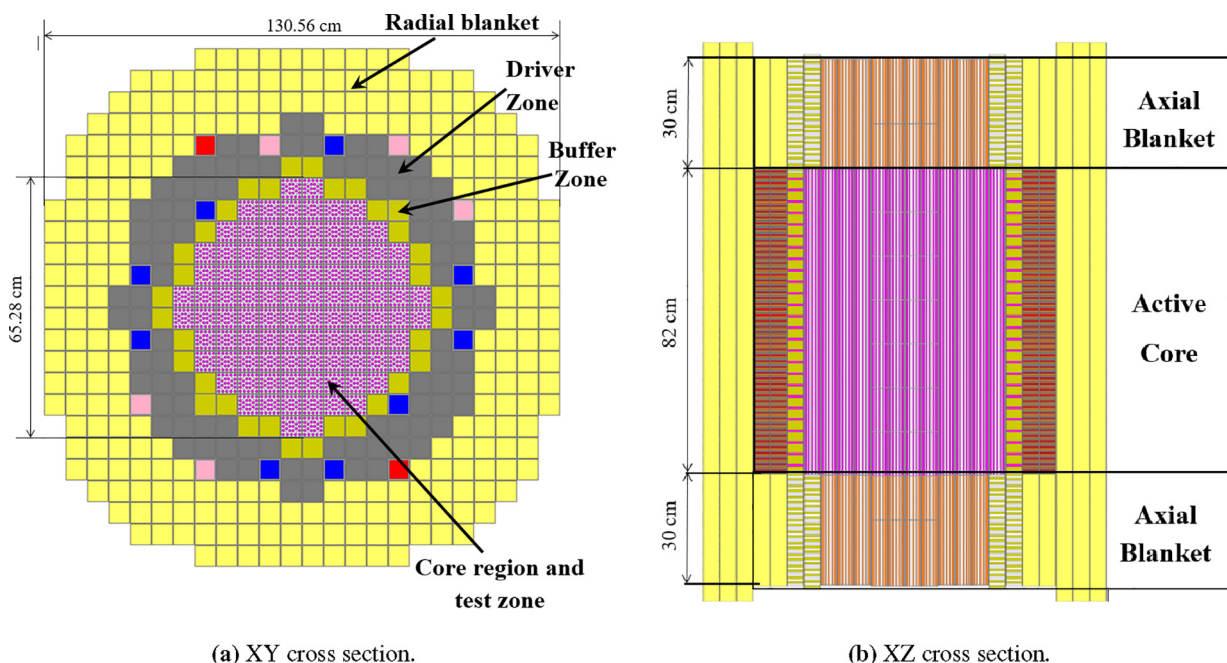


(a) XY cross section.

(b) XZ cross section.

**Fig. 1.** SNEAK-12B core layout and dimensions. The blue, red, and pink squares indicate the shim rod positions. (For interpretation of the references to color in this figure legend, the reader is referred to the web version of this article.)

conditions. The fuel cell geometry had to be designed in such a way that compaction of fuel would be possible. The full specifications of the core outline is given in Appendix A.

## 2.1. Core description

The SNEAK-12B core consists of mixed types of fuel configurations, plate and rod, and is cooled by air, which flows through the gaps between the fuel assemblies (FAs). The total core width including unused areas (filled with air) is $326.4 \times 326.4$ cm$^2$ and the total height is about 260 cm. The active core's area is $130.56 \times 130.56$ cm$^2$ and its height is about 82 cm surrounded by 30 cm of upper and lower reflectors, which make a total height of about 140 cm. The core consists of four main radial zones: a radial blanket (same as in SNEAK-12A (Margulis et al., 2017a)), a driver zone, a buffer zone, and a central core and test zone, as shown in Fig. 1. The core reactivity is controlled by 16 shim rods (marked by blue and red squares in Fig. 1a located at the driver zone region. There are several types of shim rods loaded into the core and their specification are detailed in Appendix A.5. The main

difference between the different shim rods is the axial reflector and the plate arrangement in the active region.

The fuel assemblies (bundles) are installed in a square-shaped cans of size $5.36 \times 5.36$ cm$^2$ ordered in a square grid with pitch of 5.44 cm (ensuring a gap of 0.08 cm between adjacent FAs), and at the blanket and driver zones are filled with horizontal plates. At the buffer zone and the center core the fuel assemblies contain between 13 and 39 fuel rods, where the fuel rod diameter is 0.67 cm and the cladding thickness is 0.07 cm. Representative FAs for normal loading driver zone and central core FAs are shown in Figs. 2 and 3, respectively. The blanket and axial reflector are composed of depleted uranium dioxide. The full specification of the SNEAK-12B core is given in Appendix A.

## 2.2. Experimental configurations

The number of rods per FA in the central region of the test zone depended on the specific experiment. In cases of fuel slumping-into one of the regions of the core, the number of fuel rods in that region went up to 39, as shown in Fig. 4. On the other hand, the
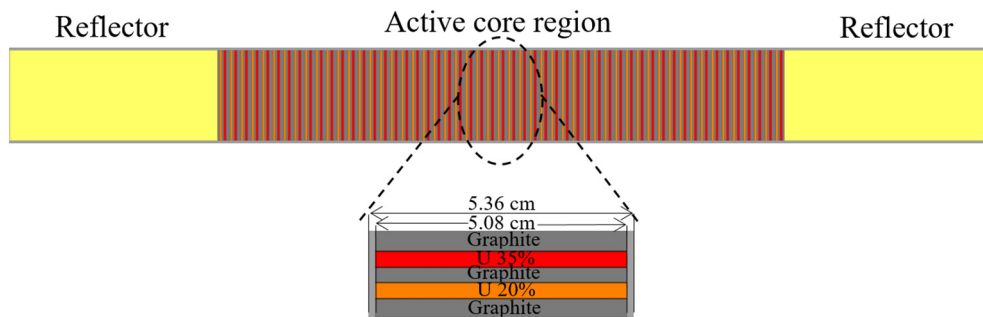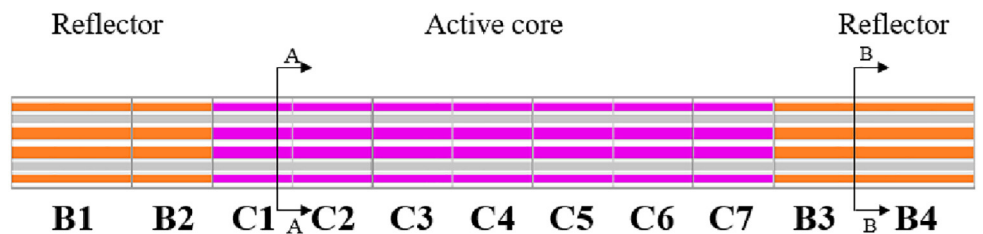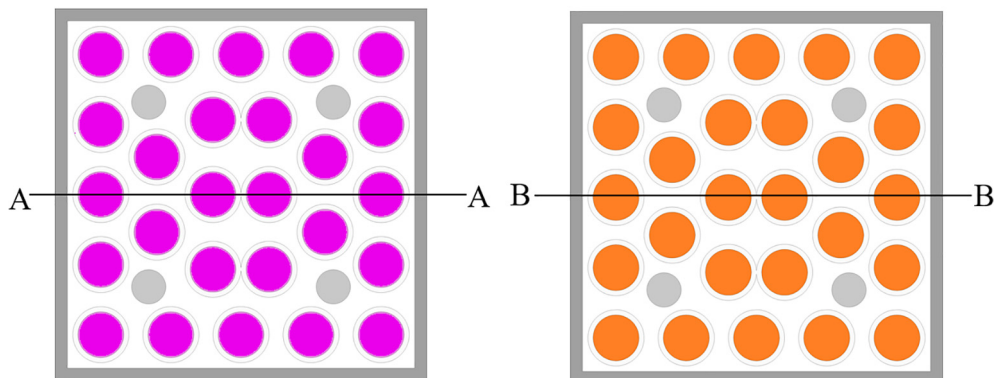


**Fig. 2.** SNEAK-12B driver zone representative fuel assembly.



**(a)** Representative fuel assembly.



**(b)** Plutonium fuel rod arrangement.

**(c)** Reflector rod arrangement.

**Fig. 3.** XZ and XY plane cross sections of a representative center core fuel assembly.
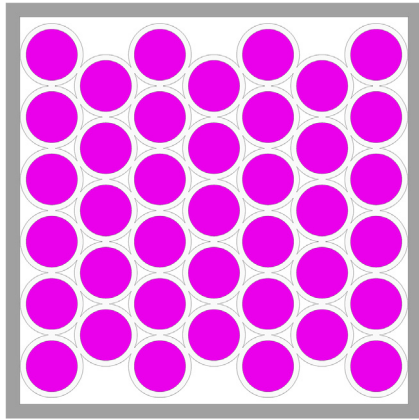
**Fig. 4.** SNEAK-12B 39 fuel rod compacted configuration.

number of fuel rods in the regions from which the fuel was relocated could vary between 13, 19 and 20 fuel assemblies (see Appendix A.7). This is achieved by removing rods from the reference configuration of 26 rods, as shown in Fig. 3b. The FA frame was stabilized by four steel support rods. In order to allow axial variation of the fuel density, the loading of the central 16 FAs was axially subdivided into 7 core segments of height of about 11 cm each (C1 to C7) and 4 axial blanket segment (B1 to B4), as shown in Fig. 3a.

Four types of SNEAK-12B experiments are analyzed:

- Fuel worth experiments – the number of rods per FA was changed in the central 1 or 4 FAs.
- Axial fuel redistribution experiments – the number of rods per FA was decreased in one axial segment and increased correspondingly in another one (in 4 or 16 FAs).
- Radial fuel redistribution experiments – fuel was displaced radially by decreasing the number of rods per FA in some FAs, and correspondingly increasing it in the neighboring FAs. The size of the modified zone varied between 12 and 48 FAs.

- Steel redistribution experiments – stainless steel was loaded into the void space between the rods of the standard FAs in 1 or 2 axial segments of 4 or 12 FAs.

Details of these experiments for axial and radial fuel movements are given in Table 1 and Fig. 5, respectively. Table 1 describes the axial layout of FAs loaded into the center of the core in each experiment. For each type of experiment, e.g., slump-out/in, the number of affected FAs is given (4, 12, or 16) and the axial structure of the FA is described. Each FA is composed of seven central axial segments of fuel (C1–C7), according to Fig. 3a, and the number of rods in each FA segment is given. The entries marked with "x" represent the standard 26 fuel pin load (Fig. 3b). Thus, for each axial segment of the FA, Table 1 provides information on the amount of loaded plutonium pins, e.g., 13, 39, 19.5. The "19.5" entries in Table 1 stand for the average amount of fuel rods, e.g., for 4 affected FAs there are two FAs with 20 fuel rods and two FAs with 19, making an average of 19.5 fuel rods per FA. The "SS" entries correspond to streaming channel blockage by stainless steel SS, i.e., the gaps between the fuel pins in the axial segment are filled with steel block. Finally, each experiment is assigned with a unique ID number given in the last column of Table 1.

The experiments of radial material redistribution are described in Fig. 5. The letters denote the different zones, i.e., "B" for blanket zone, "D" for driver zone, "F" for buffer zone, and "S" for shim rod. The blank (white) squares represent unaffected standard FAs with 26 fuel rods, whereas blank (white) squares with numbers inside denote affected FAs with a (new) number of fuel rods in them. In these experiments, the radial outward movement of fuel, the formation of central fuel-voided zone, and the accumulation of fuel around the voided zone were modeled by moving fuel rods radially outwards from central FAs to outer ones, as shown in Fig. 5(b)-(e) (ID 24–27), where the number of fuel rods drops from 26 (per FA) to 0 at the center, and the number of fuel rods is increased to 39 around the central fuel-voided zone. The last experiment, shown in Fig. 5(f) (ID 28), describes inward movement of fuel and fuel accumulation at the center of the core.

**Table 1**
Description of the axial layout of FAs loaded into the center of the SNEAK-12B core in each of the axial experiments. For each type of experiment, the number of affected FAs is given (4, 12, 16), as well as the average number of fuel rods in each axial segment (0, 13, 19.5, 39), where "x" stands for 26 fuel rods (standard FA) and "SS" stands for streaming channel blockage. Each experiment is assigned with a unique ID number. See text for more information.

| Experiment | No. of affected FAs | Description of loading (number of rods in the segment) | | | | | | | | | | | ID |
| --- | --- | --- | --- | --- | --- | --- | --- | --- | --- | --- | --- | --- | --- |
| | | B1 | B2 | C1 | C2 | C3 | C4 | C5 | C6 | C7 | B3 | B4 | |
| Slump-out | 4 | x | x | x | x | 39 | 0 | 39 | x | x | x | x | 1 |
| | 16 | | | | | | | | | | | | 2 |
| | 4 | x | x | 39 | x | x | 0 | x | x | 39 | x | x | 3 |
| | 16 | | | | | | | | | | | | 4 |
| | 4 | x | x | x | x | x | 0 | x | x | 39 | 39 | x | 5 |
| | 16 | | | | | | | | | | | | 6 |
| Slump-in | 4 | x | x | x | x | 19.5 | 39 | 19.5 | x | x | x | x | 7 |
| | 16 | | | | | | | | | | | | 8 |
| | 4 | x | x | 19.5 | x | x | 39 | x | x | 19.5 | x | x | 9 |
| | 16 | | | | | | | | | | | | 10 |
| | 4 | x | x | 0 | x | x | 39 | 39 | x | x | x | x | 11 |
| | 16 | | | | | | | | | | | | 12 |
| Slump-through | 4 | x | x | 13 | x | x | x | x | x | 39 | x | x | 13 |
| | 16 | | | | | | | | | | | | 14 |
| | 16 | x | x | 13 | 13 | x | x | x | 39 | 39 | x | x | 15 |
| Steel insertion | 4 | x | x | SS | x | x | x | x | x | SS | x | x | 16 |
| | 4 | x | x | x | x | x | x | x | x | SS | SS | x | 17 |
| | 12 | x | x | x | x | x | SS | x | x | x | x | x | 18 |
| | 12 | x | x | x | x | x | x | x | x | SS | x | x | 19 |
| Large axial move | 12 | x | x | x | x | 0 | 0 | 39 | 39 | 39 | 39 | x | 20 |
| | 12 | x | 39 | 39 | 39 | 0 | 0 | 0 | 39 | 39 | 39 | x | 21 |
| | 12 | x | x | 0 | 0 | 39 | 39 | 39 | 39 | x | x | x | 22 |
| | 12 | x | 39 | 0 | 0 | 0 | 39 | 39 | 39 | 39 | 39 | x | 23 |

**(a)** Clear 0 (0).

**(b)** Out 4 (8) ID-24.

**(c)** Out 9 (18) ID-25.

**(d)** Out 12 (24) ID-26.

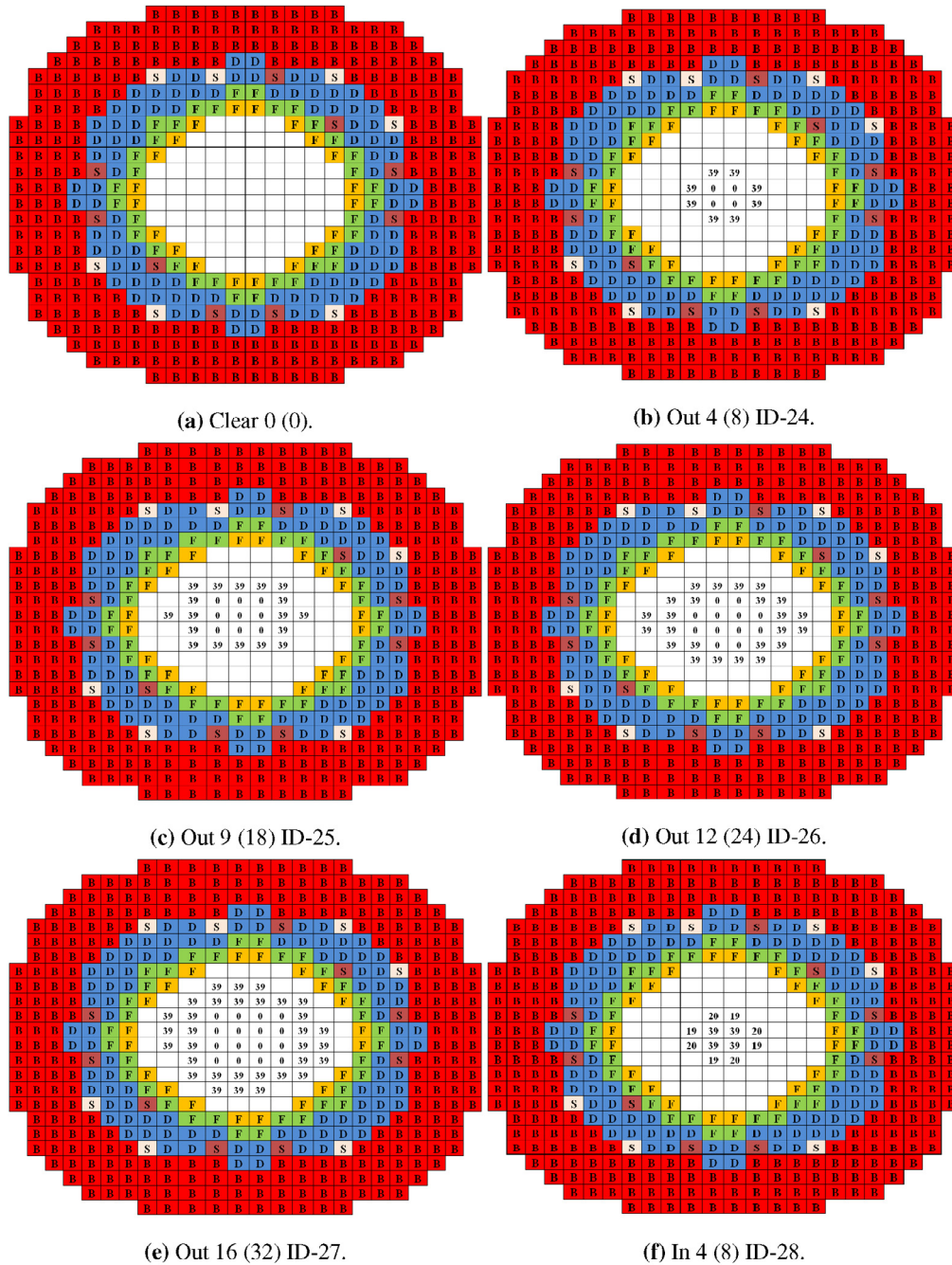**(e)** Out 16 (32) ID-27.

**(f)** In 4 (8) ID-28.

**Fig. 5.** Description of the radial material redistribution experiments. The letters denote the different zones, i.e., "B" for blanket zone, "D" for driver zone, "F" for buffer zone, and "S" for shim rod. The blank (white) squares represent unaffected standard FAs with 26 fuel rods, whereas blank (white) squares with numbers inside denote affected FAs with a (new) number of fuel rods in them. The radial outward movement of fuel was modeled by moving fuel rods radially outwards from central FAs to outer ones, as shown in panels (b)-(e) (ID 24–27), where panel (f) (ID 28) describes inward movement of fuel. The caption denotes whether fuel was moved outwards/inwards, the number of FAs with reduced/increased amount fo fuel, respectively, and the total number of affected FAs.

The multiplication factor estimation is inferred from doubling time measurements with a given Nordheim curve. However, no additional information on the delayed neutron fractions was given for the analysis. The reactivity effects were measured by compensation using shim rod calibration in the SNEAK-12 core. By repeating experiments, the accuracy of the shim rod worth is estimated to be about 0.2 cents (Henneges, 1988).

## 3. Computational tools

Reactivity variations between different experimental configurations studied in this work are compared to results obtained by

Monte Carlo (MC) codes (MCNPX2.7 (X-5 Monte Carlo Team, 2003) and Serpent-2.1.29 (Leppanen et al., 2015)) and by the ERA-NOS 2.4 reference deterministic transport code (Ruggieri et al., 1973). The nuclear data library used in this study is based on the JEFF-3.1.1 evaluation (Santamarina et al., 2009). For each configuration, a two-dimensional (R-Z) ERANOS model has been developed and transport calculations were performed by employing the self-shielded neutron cross-section processed at 33 energy groups by means of the European Cell COde ECCO (Ruggieri et al., 1973), which is part of the ERANOS package. This 33-energy mesh, adequate for fast systems, is derived from the international X-MAS 172-energy structure (Sartori et al., 1990). The MC calculations are

done in three-dimensional geometries as specified by the SNEAK-12B benchmark. The calculations are performed based on 200,000 neutron histories with 5000 active and 500 inactive cycles, such as to guarantee a convergence on the $k_{eff}$ of less than 10 pcm and less than 1% on local flux distributions (a fuel assembly scale).

### 3.1. Few-group cross-section generation for ERANOS

Unlike the SNEAK-12A core, which consists of vertically stacked plates (Margulis et al., 2017a), the SNEAK-12B has different combinations of fuel rod geometries (Appendix A.7), as discussed in previous sections. This presents some challenges for cross-section homogenization due to the limitation of geometry definition in ECCO cell. ECCO allows two types of fuel lattice arrangement, square and hexagonal, none of which are compatible with the lattice arrangements in SNEAK-12B fuel bundles. Therefore, equivalent assemblies are defined by conservation of fissile material loading, assembly volume, and (whenever possible) the actual amount of fuel rods in the original SNEAK-12B FAs (26 and 39 FAs) in order to ensure that the self-shielding calculation are not affected (in the case of ERANOS calculations).

In ERANOS, effective microscopic and macroscopic cross-sections are computed by the ECCO cell code. ECCO generates multigroup self-shielded cross-sections and elastic, inelastic, and N,xN group-to-group transfer cross-section for core calculations in ERANOS. ECCO solves the integral transport equation in an infinite lattice, using multigroup cross-sections with a fine energy group structure (1968 groups, which extends up to 20 MeV) and as accurate as possible geometrical representation. ECCO then condenses the fine-group structured cross-sections into a 33-group structure. In this work, the cross-section homogenization assumed the critical B1 model.

In order to generate few-groups homogenized cross section for the 26 fuel rod assembly (Fig. 3a) a representative model of 25 fuel rods was created for ECCO cell, as show in Fig. 6a. The representative square lattice in ECCO is characterized by slightly bigger fuel rod (original rod radius 0.335 cm, modified rod radius 0.342 cm). The same approach was applied for the 39 rods geometry had to be transformed into a hexagonal model with 37 rods, as shown in Fig. 6b. This change should conserve the different reaction rates in each fuel assembly.

The few-group homogenized cross-sections and reaction rates generated using Serpent and ECCO models exhibit good agreement for the 26/25 pin model, as shown in Fig. 7, and the 39/37 pin model as show in Fig. 8. The discrepancies in the low energy range (below $10^{-2}$ MeV) can be disregarded due to the negligible amount of neutrons in those energies, as indicated by the flux spectrum for the two models (26 pin model Fig. 7 and 39 pin model Fig. 8).

Generally, whenever an equivalent model needs to be defined, one must decide on the physical quantities to be conserved. This is usually a trade-off decision, because conservation of one physical quantity usually comes at the expense of another. For example, in cross-section homogenization, it is impossible to conserve all together the average node flux, the surface fluxes, the reaction rates, and the flux's continuity at the node's surfaces. The same applies in this case. The above equivalent models are designed to conserve the most important physical quantity in this case, which are the total fission and capture reaction rate. Although the change in the pin dimension change quantities such as the Dancoff and Bell factors, which in turn affect the spatial self-shielding, their effect on the total reaction rates remain small due to the fast spectrum and the large neutron mean free path characterizing the SNEAK-12B core.

The differences between the flux spectra of the equivalent 37 pins model in ECCO with respect to the reference 39 and 37 pins models in Serpent reach up to 30%/10%, respectively, as shown in Fig. 8. This leads to an approximate 20% difference in the fission and capture cross-section calculated using the equivalent 37 pins model in ECCO with respect to the ones calculated by the reference 39 pins model in Serpent. The differences between the fission and capture cross-section calculated using the equivalent 37 pins model in ECCO and the ones calculated by the reference 37 pins model in Serpent are negligible. These comparisons are shown in Fig. 8 for fission and capture, respectively. However, the total reaction rates are in well agreement for the different models, as shown in Fig. 8 for fission and capture, respectively. The equivalent models for ECCO yield an agreement between full core calculations by ERANOS and Serpent, as demonstrated in the following section.

## 4. Results

In this section, measured and calculated results are compared. In order to obtain an indication for the accuracy of the different codes, results from all different experimental and numerical methods are cited. The effective neutron multiplication factor $k_{eff}$ estimation in the SNEAK-12 experiments was inferred from doubling time measurements with a given Nordheim curve. However, no additional information on the delayed neutron fraction was given.
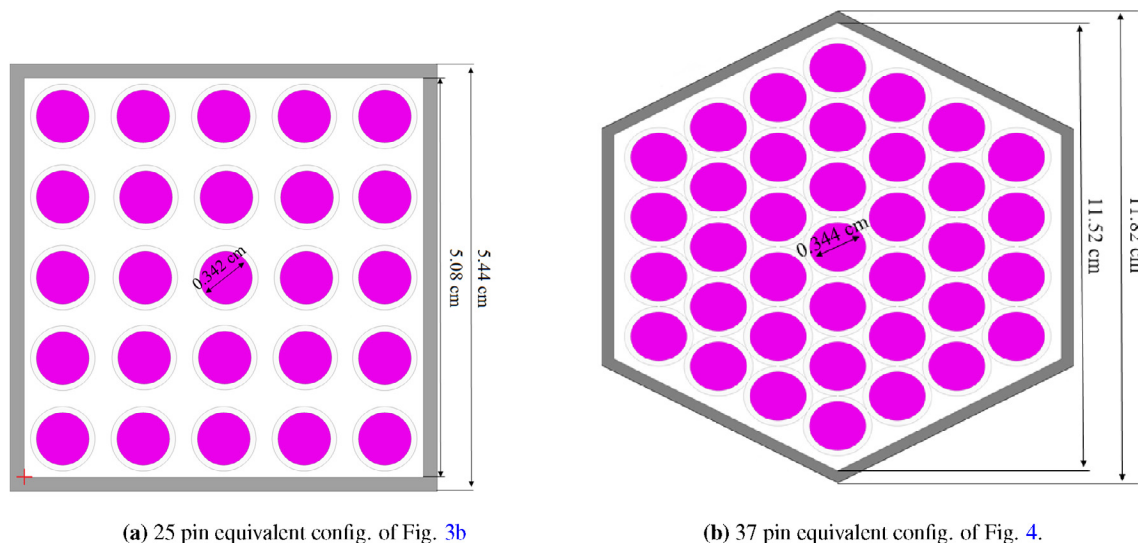


**(a)** 25 pin equivalent config. of Fig. 3b

**(b)** 37 pin equivalent config. of Fig. 4.

**Fig. 6.** ECCO cell equivalent rod configurations of the original SNEAK-12B rod bundles configuration for cross-section calculation.
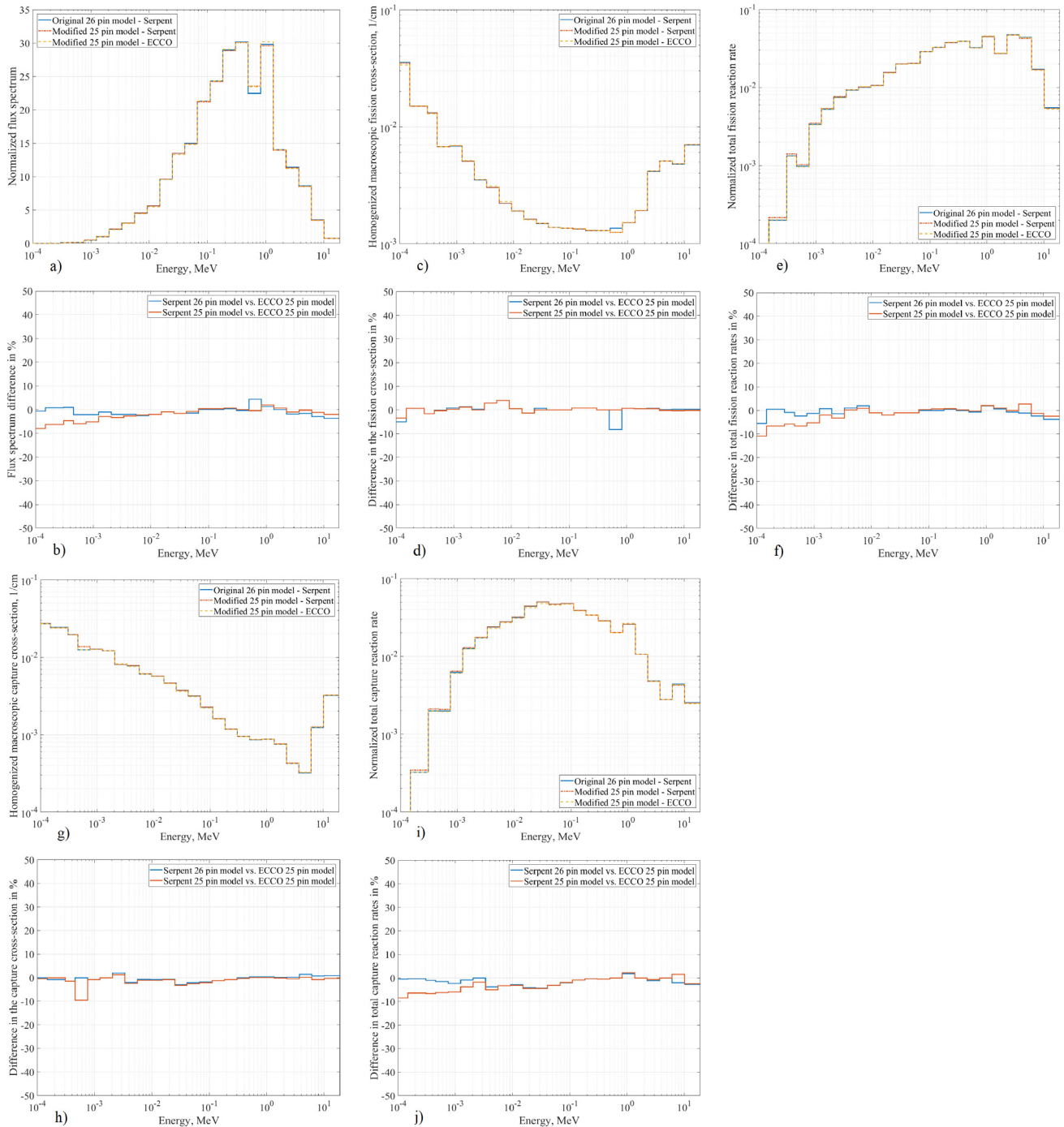
**Fig. 7.** Comparison of the equivalent ECCO model and the reference Serpent model for 26 pin assembly.

## 4.1. Clear criticality experiment

The different experiments considered in this section are all referenced to the most basic unperturbed (clear) core loading of SNEAK-12B (the reference core). Therefore, it is essential to correctly calculate the reference core. The experimental versus calculated values of the effective multiplication factor $k_{eff}$ are summarized in Table 2. The agreement between the different codes and the experimental values is excellent. The ERANOS R-Z model deviates from the experimental result by about 150 pcm, which is a result of the cylindrical geometry approximation and high heterogeneity of the core. However, this deviation is lower than the deviation of the R-Z model in comparison to the SNEAK-12A experiments (~600 pcm) (Margulis et al., 2017a).

Unfortunately, there is almost no available data for comparison except the core effective multiplication factor and the reactivity changes between the different configurations. This is due to lack of miniature measurement equipment that could have been fitted inside the tight core arrangement of the SNEAK-12. Therefore, a comparison of flux traverses and reaction rates distribution for the clear core configuration is made only between the different codes. The agreement between the different codes on the integrated axial flux distribution along the core center line is excellent, as shown in Fig. 9.
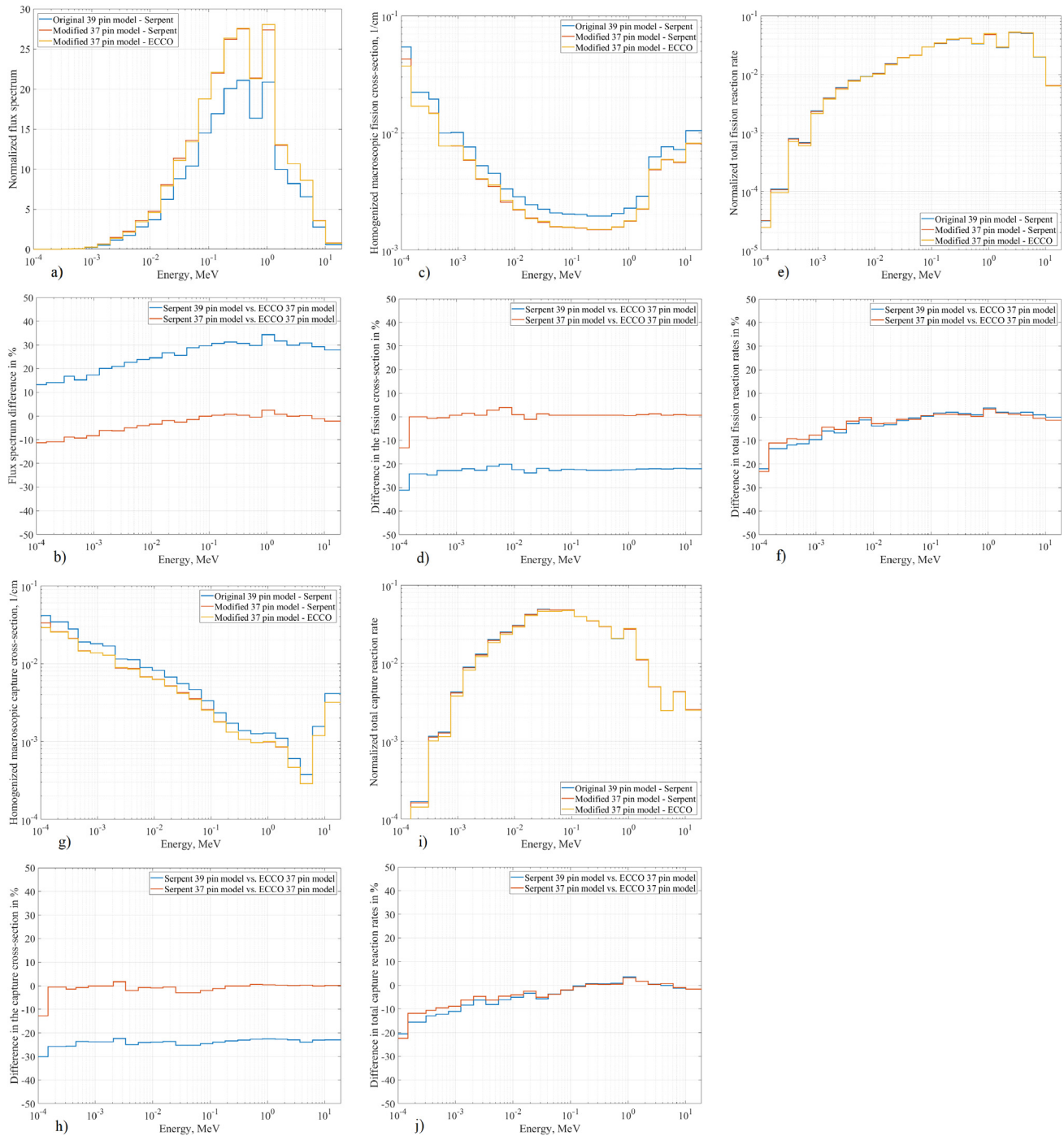
**Fig. 8.** Comparison of the equivalent ECCO model and the reference Serpent model for 39 pin assembly.

**Table 2**
Comparison of the effective multiplication factor obtained from the experiment and the different codes for the basic unperturbed (clear) configuration of SNEAK-12B.

| Source | $k_{\text{eff}}$ | Diff. from experiment, pcm |
|---|---|---|
| Experimental | $1.00127 \pm 1.5E - 04$ | – |
| Serpent 2.1.29 | $1.00105 \pm 3E - 05$ | $-22.1$ |
| MCNPX2.7 | $1.00158 \pm 2E - 05$ | $30.7$ |
| ERANOS 2.4 (R–Z) | $0.99957$ | $-170$ |

The spatial distribution of the neutrons energy spectrum, calculated by Serpent in 33 energy groups, is shown in Fig. 10. In Fig. 10a, the normalized flux spectrum (z-axis) is plotted for each radial position (x-axis) and for each energy group range (y-axis). An explicit spatial cross-section of the flux (i.e., along the x-axis) at two distinct energy groups is shown in Fig. 10b. The two energy groups are chosen to represent two distinct behaviors of the neutron flux. Two observations are should be outlined. First, the spectrum at the driver zone is harder than the spectrum in the test zone, as clearly shown by examining energy group 26 (0.3–0.5 MeV) in Fig. 10b. This is due to the presence of plutonium and uranium in the buffer and driver zones. Clearly this is not the situation for slower neutrons (represented by energy group 20, 0.015–0.025 MeV). Second, the flux in the test zone remains fairly homogeneous (flat) for all energy groups up to the radial interface with the buffer zone. This is clearly demonstrated by

the spatial flux distribution of the two representative energy groups (Fig. 10b). It should be noted that the homogeneity of the radial distribution of the integral flux throughout the test zone is less representative of FBRs. However, when studying spatial relocation of fuel in the test zone, the homogeneity of the flux in the unperturbed test zone eliminates any experimental biases due to spatial gradients of the flux and enables the evaluation of reactivity effects solely due to fuel relocation.

### 4.2. Steel blockage results

In these experiments the space between the fuel rods was filled with Stainless Steel (SS) at the locations specified in Table 1 (exper-
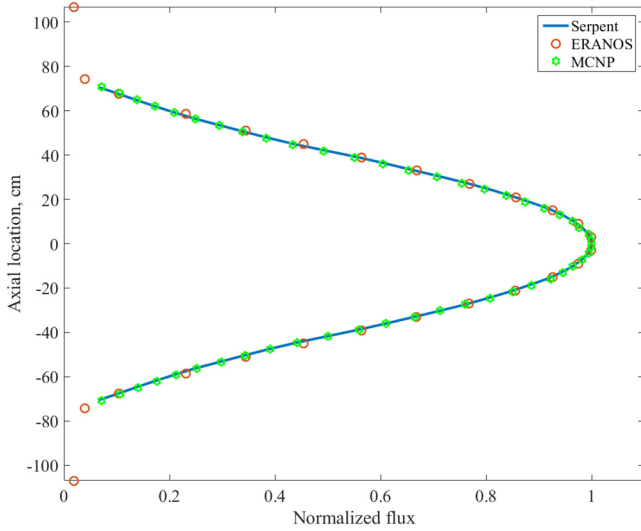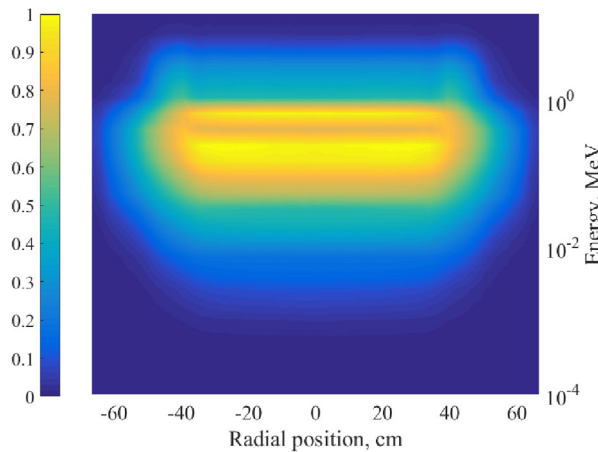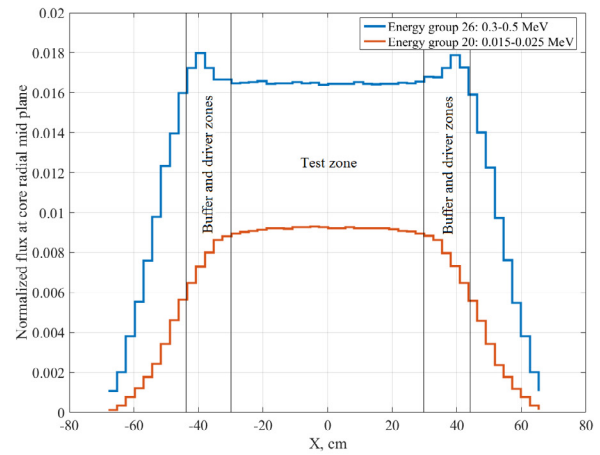
**Fig. 9.** Comparison of integrated axial flux distribution at core center line obtained by different codes.

iment IDs 16–19). The purpose of these experiments was to investigate the blockage of local streaming channels by SS. The results for these experiments are summarized in Table 3 and illustrated in Fig. 11. These results include the reactivity changes with respect to the clear criticality experiment and the difference between the different codes. The results indicate a large reactivity loss when steel is introduced into the core center. This reactivity loss is mainly due to increased scattering introduced by the SS, which increases the removal of neutrons from a high neutron importance region (the core center) to lower importance regions. On the other hand, the introduction of SS at the core boundaries leads to reactivity gain due to increase in axial reflector efficiency.

According to Table 3 and Fig. 11, the calculated results are consistently higher than the experimental ones. This is probably due to the inconsistency between the steel type utilized by the simulations (SS316) and the actual steel used in the experiments. Unfortunately, the material balance of the actual steel was not found in the records. Nonetheless, the overall simulation results are similar to the experimental data.

### 4.3. Axial fuel redistribution results

Several different configurations were examined through the experimental program, as summarized in Table 1 experiment IDs 1–15 and 20–23. The slump-in and slump-out case involve three axial sections in 4 or 16 central affected bundles. These experiments include symmetric fuel movement over short and long distances, and asymmetric redistribution of fuel with some fuel relocated into the axial blanket. Additional experiments involve large scale material relocation of different parts of the 12 center bundles.

The reactivity changes caused by axial redistribution of fuel are the dominating neutronic effects, which would determine the course of a SCA progression. The axial redistribution experimental and calculated results are summarized in Table 4 and illustrated in Fig. 12. The differences between the reactivity changes calculated

**(a)** 33 energy groups.

**(b)** 2 energy groups.

**Fig. 10.** Normalized flux spectrum distribution for the clear core configuration.

**Table 3**
Steel blockage results (in cents).

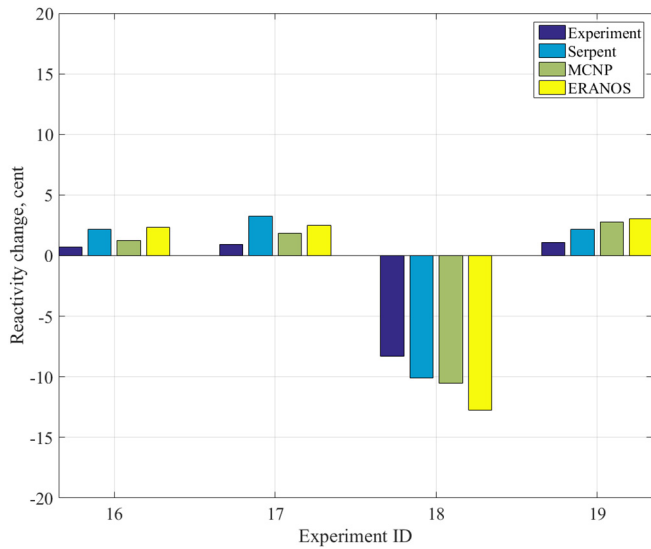| Exp. ID | Experimental | $\Delta\rho_{Serpent}$ | $C_{Serpent}$-E | $\Delta\rho_{MCNPX}$ | $C_{MCNPX}$-E | $\Delta\rho_{ERANOS}$ | $C_{ERANOS}$-E |
|---|---|---|---|---|---|---|---|
| 16 | $0.70 \pm 0.2$ | $2.17 \pm 0.47$ | $1.47 \pm 0.51$ | $1.24 \pm 0.31$ | $0.54 \pm 0.40$ | 2.35 | 1.65 |
| 17 | $0.90 \pm 0.2$ | $3.25 \pm 0.47$ | $2.35 \pm 0.51$ | $1.86 \pm 0.31$ | $0.96 \pm 0.40$ | 2.48 | 1.58 |
| 18 | $-8.30 \pm 0.2$ | $-10.07 \pm 0.47$ | $-1.77 \pm 0.51$ | $-10.53 \pm 0.31$ | $-2.23 \pm 0.40$ | -12.76 | -4.46 |
| 19 | $1.10 \pm 0.2$ | $2.17 \pm 0.47$ | $1.07 \pm 0.51$ | $2.79 \pm 0.31$ | $1.69 \pm 0.40$ | 3.06 | 1.96 |

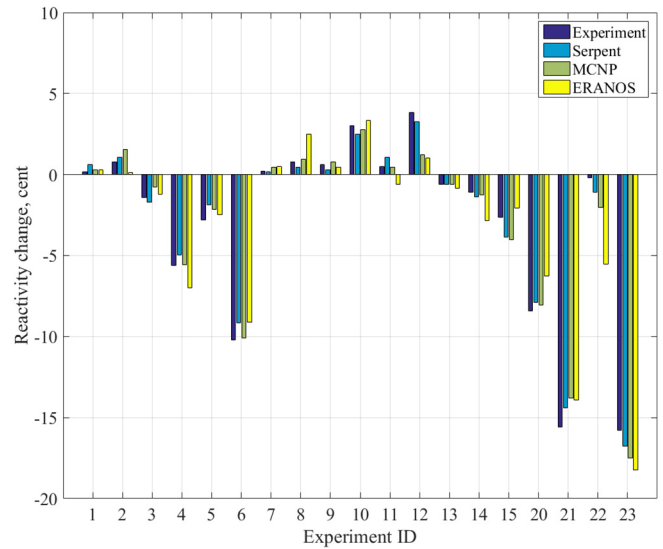Fig. 11. Reactivity changes due to stainless steel addition.



Fig. 12. Reactivity changes due to axial fuel movement.

by Serpent, MCNPX and ERANOS are very small (below 20 pcm). The results obtained by Serpent and MCNPX compare well with the experimental results. The results obtained by ERANOS also compare well with the experimental values, excluding the asymmetric slump-in (experiment ID 11–12) and large vertical movements (experiment ID 22–23). This could be the result of an incorrect estimation of the leakage factor (Tommasi et al., 2010).

Nevertheless, the capabilities of the MC codes to reproduce the experimental values are excellent. Some axial fission rate distributions were obtained by traverse measurements using different fission chambers. Unfortunately, these measurements are not available except for a single representation, which is shown in Fig. 13a (Henneges, 1988). The data presented in Fig. 13a was digitized using WebPlotDigitizer software (Rohatgi, 2018), which enables the extraction of numerical data from images of data visualization. The error associated with the digitization is conservatively estimated by 2% of each digitized point value for each curve. Unfortunately, there is no available date regarding the experimental uncertainty of the fission rate distribution.

The axial distributions of fission rate in $^{239}$Pu and $^{238}$U calculated by Serpent are compared to the measured ones in Fig. 13b and show good agreement with slight deviations in the upper reflector region. This might be the result of small neutron flux in this region due to fuel slump towards the bottom of the core. Additional comparison of one energy group integrated axial flux distribution along the core center line between Serpent, MCNPX and ERANOS for two experiments is shown in Fig. 14. The experiments compared are the large asymmetric slump (ID-12) and the large axial fuel movement (ID-22).

The two cases considered in Fig. 14 show a slight deviation of the flux obtained from ERANOS towards the upper part of the core. This is due to unavoidable modifications in the ERANOS model due to geometry restrictions in the geometry input options (i.e., global mesh encapsulating all zones). The nodes height in ERANOS was dictated by the most basic unit cell, which is the driver zone cell 12B/N (Fig. A.3a) with total height of about 1.5 cm. The test zone axial segment is 11.75 cm in height, meaning that it can contain ~7.5 12B/N cells, which was rounded to 8 in order to conserve an integral number of unit cells. This nodalization compromise leads to a slightly increased amount of fissile material in the com-

**Table 4**
Axial fuel redistribution results (in cents).

| Exp. ID | Experimental | $\Delta\rho_{Serpent}$ | $C_{Serpent}$–E | $\Delta\rho_{MCNPX}$ | $C_{MCNPX}$–E | $\Delta\rho_{ERANOS}$ | $C_{ERANOS}$–E |
|---|---|---|---|---|---|---|---|
| 1 | 0.15 ± 0.2 | 0.62 ± 0.47 | 0.47 ± 0.51 | 0.31 ± 0.31 | 0.16 ± 0.40 | 0.29 | 0.14 |
| 2 | 0.80 ± 0.2 | 1.08 ± 0.47 | 0.28 ± 0.51 | 1.55 ± 0.31 | 0.75 ± 0.40 | 0.14 | −0.66 |
| 3 | −1.40 ± 0.2 | −1.70 ± 0.47 | −0.30 ± 0.51 | −0.77 ± 0.31 | 0.63 ± 0.40 | −1.21 | 0.19 |
| 4 | −5.60 ± 0.2 | −4.96 ± 0.47 | 0.64 ± 0.51 | −5.57 ± 0.31 | 0.03 ± 0.40 | −6.99 | −1.39 |
| 5 | −2.80 ± 0.2 | −1.86 ± 0.47 | 0.94 ± 0.51 | −2.17 ± 0.31 | 0.63 ± 0.40 | −2.49 | 0.31 |
| 6 | −10.20 ± 0.2 | −9.14 ± 0.47 | 1.06 ± 0.51 | −10.07 ± 0.31 | 0.13 ± 0.40 | −9.12 | 1.08 |
| 7 | 0.20 ± 0.2 | 0.15 ± 0.47 | −0.05 ± 0.51 | 0.46 ± 0.31 | 0.26 ± 0.40 | 0.48 | 0.28 |
| 8 | 0.80 ± 0.2 | 0.46 ± 0.47 | −0.34 ± 0.51 | 0.93 ± 0.31 | 0.13 ± 0.40 | 2.48 | 1.68 |
| 9 | 0.60 ± 0.2 | 0.31 ± 0.47 | −0.29 ± 0.51 | 0.77 ± 0.31 | 0.17 ± 0.40 | 0.47 | −0.13 |
| 10 | 3.00 ± 0.2 | 2.48 ± 0.47 | −0.52 ± 0.51 | 2.79 ± 0.31 | −0.21 ± 0.40 | 3.36 | 0.36 |
| 11 | 0.50 ± 0.2 | 1.08 ± 0.47 | 0.58 ± 0.51 | 0.46 ± 0.31 | −0.04 ± 0.40 | −0.60 | −1.10 |
| 12 | 3.85 ± 0.2 | 3.25 ± 0.47 | −0.60 ± 0.51 | 1.24 ± 0.31 | −2.61 ± 0.40 | 1.02 | −2.83 |
| 13 | −0.60 ± 0.2 | −0.62 ± 0.47 | −0.02 ± 0.51 | −0.62 ± 0.31 | −0.02 ± 0.40 | −0.84 | −0.24 |
| 14 | −1.10 ± 0.2 | −1.39 ± 0.47 | −0.29 ± 0.51 | −1.24 ± 0.31 | −0.14 ± 0.40 | −2.84 | −1.74 |
| 15 | −2.65 ± 0.2 | −3.87 ± 0.47 | −1.22 ± 0.51 | −4.03 ± 0.31 | −1.38 ± 0.40 | −2.06 | 0.59 |
| 20 | −8.40 ± 0.2 | −7.90 ± 0.47 | 0.50 ± 0.51 | −8.05 ± 0.31 | 0.35 ± 0.40 | −6.28 | 2.12 |
| 21 | −15.60 ± 0.2 | −14.41 ± 0.47 | 1.19 ± 0.51 | −13.79 ± 0.31 | 1.81 ± 0.40 | −13.93 | 1.67 |
| 22 | −0.20 ± 0.2 | −1.08 ± 0.47 | −0.88 ± 0.51 | −2.01 ± 0.31 | −1.81 ± 0.40 | −5.53 | −5.33 |
| 23 | −15.80 ± 0.2 | −16.77 ± 0.47 | −0.97 ± 0.51 | −17.51 ± 0.31 | −1.71 ± 0.40 | −18.21 | −2.41 |

**(a)** Original [4].

**(b)** Serpent vs. experimental digitized data.

**Fig. 13.** Fission chamber traverse results for the asymmetric slump-out experiment (ID 15).



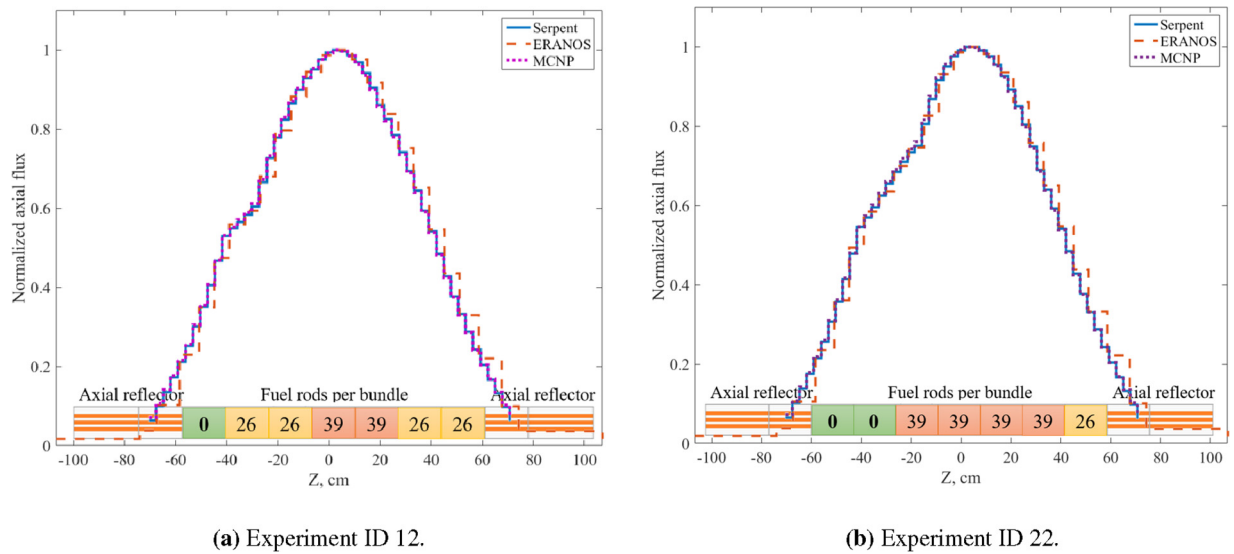**(a)** Experiment ID 12.

**(b)** Experiment ID 22.

**Fig. 14.** Comparison of axial flux distribution along the core center line calculated using Serpent, ERANOS, and MCNPX.

**Table 5**
Radial fuel redistribution results (in cents).

| Exp. ID | Experimental | $\Delta\rho_{Serpent}$ | $C_{Serpent}$-E | $\Delta\rho_{MCNPX}$ | $C_{MCNPX}$-E | $\Delta\rho_{ERANOS}$ | $C_{ERANOS}$-E |
|---------|--------------|------------------------|-----------------|----------------------|---------------|-----------------------|----------------|
| 24 | −4.90 ± 0.2 | −4.80 ± 0.47 | 0.10 ± 0.51 | −5.42 ± 0.31 | −0.52 ± 0.40 | 3.01 | 7.91 |
| 25 | −12.00 ± 0.2 | −11.78 ± 0.47 | 0.22 ± 0.51 | −13.17 ± 0.31 | −1.17 ± 0.40 | −8.29 | 3.71 |
| 26 | −14.70 ± 0.2 | −15.65 ± 0.47 | −0.95 ± 0.51 | −15.65 ± 0.31 | −0.95 ± 0.40 | −16.84 | −2.14 |
| 27 | −19.10 ± 0.2 | −19.24 ± 0.47 | −0.14 ± 0.51 | −18.60 ± 0.31 | −0.50 ± 0.40 | −27.60 | −8.50 |
| 28 | −1.60 ± 0.2 | −1.39 ± 0.47 | 0.21 ± 0.51 | −1.55 ± 0.31 | 0.05 ± 0.40 | −0.43 | 1.17 |

pacted configuration in ERANOS, resulting in the small deviation observed in Fig. 14. Overall, the agreement between the results is good with slight deviation towards the core edges.

### 4.4. Radial fuel redistribution

The radial redistribution of fuel from the central region to the test zone periphery is illustrated in Fig. 5. The size of the voided area varies from 4 to 16 fuel assemblies over the entire active core height (C1 to C7). Additionally, a single fuel radial slump-in config-

uration was examined (Fig. 5f). For these experiments long fuel bundles were used in the core center.

The measured and calculated values are summarized in Table 5 and illustrated in Fig. 15. The measured reactivity changes are small and negative. The Serpent and MCNPX results are in good agreement with the experiment, and the ERANOS results show relatively large deviations. The deviations of ERANOS results with respect to the experimental values are due to the large number of voided areas in the core center, which lead to incorrect estimation of leakage factors. Similar behavior was observed in the
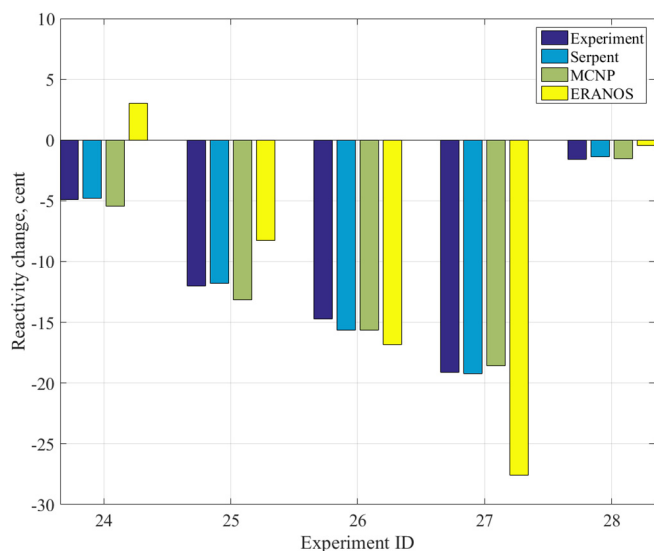
**Fig. 15.** Reactivity changes due to radial fuel movement.

SNEAK-12A analysis in radial fuel movement (Margulis et al., 2017a).

The negative reactivity changes in the slump-out experiments (ID 24–27) are expected. However, the negative reactivity change in the slump-in experiment (ID 28) is surprising. It may be attributed to the fact the fuel is moved along a near-zero gradient in the flux combined with voided regions that increase the leakage term. Nevertheless, the maximal reactivity measurement was of −20 cents. These experiments gave rise to the maximal deviation between Serpent and ERANOS.

## 5. Conclusions

This paper presents a revaluation of the second campaign of the SNEAK-12 program. In the first evaluation of the SNEAK-12A core, a single-zone uranium-fueled critical assembly loaded with enriched $^{235}U$ plates (Margulis et al., 2017a) was examined. However, the utilization of uranium in the SNEAK-12A core was not representative of an actual fuel to be loaded in a future fast reactors. Therefore, it was necessary to investigate whether the findings made in SNEAK-12A are applicable for $PuO_2UO_2$ based fuels. The latter is the main goal of this paper.

The benchmark results constitute a solid basis of knowledge in order to study neutronics behavior of distorted configuration in fast reactor cores. Currently, efforts are ongoing to carry out similar analyses for other fast reactor systems.

The SNEAK-12B core was loaded with plutonium rods lattices. The reactivity changes found in the SNEAK-12B were small with respect to SNEAK-12A. Axially-wise, this is probably due to the fact that axial fuel redistribution was possible only in the center 16 bundles. Radially-wise, this is probably due to the almost constant flux in the core center, as shown in Fig. 10. For example, large flux gradients existed in the SNEAK-12A core gave rise to reactivity changes on the order of dollars.

A summary of experimental configurations is given in Table 1 and Fig. 5 and the experimental and calculations results are given in Tables 3–5 and in Figs. 11–13, and 15. Generally, the calculation results by ERANOS, MCNPX and Serpent show good agreement with the experimental results and between themselves. This is partially attributed to the adoption of equivalent models for ECCO cell calculations, for which an example is shown in Fig. 6. However, for some configurations ERANOS results show deviations, which could

be associated with the high level of heterogeneity of the core configuration leading to under estimation of the leakage factor.

This is the last piece in the re-examination of the SNEAK-12B experiment. A comprehensive nuclear data sensitivity and uncertainty analysis of the reactivity coefficients as well as $k_{eff}$ due to fuel redistribution and associated nuclear data propagated uncertainties was carried out and published in a complementary paper (Margulis et al., 2018).

The better understanding of past experiments, provided by this benchmark, introduce additional information and physical knowledge for future experimental programs at CEA Cadarache, in particular the awaited innovative ZPR design such as the ZEPHYR project currently under development and led by CEA.

## Appendix A. Supplementary material

Supplementary data associated with this article can be found, in the online version, at https://doi.org/10.1016/j.anucene.2018.09.025.

## References

Blaise, P., Boussard, F., Ros, P., Leconte, P., Margulis, M., Martin, G., Blandin, K., 2016. Advanced small and large core distortion modeling in ZPR to assess core recriticality scenarios of SFR core degradation sequences. In: Proc. Int. Conf. IGORR-2016. European Nuclear Society, Berlin Germany.

Brun, E., Damian, F., Diop, C.M., Dumonteil, E., Hugot, F.X., Jouanne, C., Lee, Y.K., Malvagi, F., Mazzolo, A., Petit, O., Trama, J.C., Visonneau, T., Zoia, A., 2015. TRIPOLI-4, CEA, EDF and AREVA reference Monte Carlo code. Ann. Nucl. Energy 82, 151–160.

Devictor, N., 2013. R&D challenges for SFR design and safety analysis – opportunities for internationall cooperation. In: Proc. Int. Conf. on Fast Reactors and Related Fuel Cycles – FR13. IAEA, Paris, France.

Helm, F., 1996. The SNEDAX Data Base – General Description and Users Instruction. Tech. Rep. Forschungszentrum Karlsruhe, Karlsruhe, Germany.

Helm, F., Henneges, G., 1985. Measurements and calculation of reactivity effects of material rearrangements in a plutonium-fueled fast reactor rod lattice. Nucl. Technol. 71, 68–81.

Helm, F., Henneges, G., Maschek, W., 1984. Measurements and computation of the reactivity effects of accident-caused core distortions in Liquid-Metal Fast Breeder Reactors. Nucl. Sci. Eng. 87, 295–313.

Henneges, G., 1988. Validation of neutronic codes for distorted core configurations with the SNEAK-12 critical assemblies. Nucl. Sci. Eng. 100, 314–323.

Leppanen, J., Pusa, M., Viitanen, T., Valtavirta, V., Kaltiaisenaho, T., 2015. The Serpent Monte Carlo code: status, development and applications in 2013. Ann. Nucl. Energy 82, 142–150.

Margulis, M., Blaise, P., Gabrielli, F., Gruel, A., Mellier, F., Gilad, E., 2017a. The path for innovative severe accident neutronics studies in ZPRs. Part I. 1 – Analysis of SNEAK-12A experiments for core disruption in LMFBRs. Prog. Nucl. Energy 94, 106–125.

Margulis, M., Blaise, P., Mellier, F., Gilad, E., 2017b. The path for innovative severe accident neutronics studies in ZPRs. Part I. 2 – Impact of nuclear data uncertainties on reactivity changes of SNEAK-12A core. Prog. Nucl. Energy 96, 97–117.

Margulis, M., Blaise, P., Gilad, E., 2018. Modeling representative Gen-IV molten fuel reactivity effects in the ZEPHYR fast/thermal coupled ZPRs. Part I – Assembly level. Int. J. Energy Res. 42 (5), 1950–1972. Available from: arXiv:<https://onlinelibrary.wiley.com/doi/pdf/10.1002/er.3991>. https://doi.org/10.1002/er.3991. <https://onlinelibrary.wiley.com/doi/abs/10.1002/er.3991>.

Margulis, M., Blaise, P., Mellier, F., Gilad, E., 2018. The path for innovative severe accident neutronics studies in ZPRs. Part II.2 – Impact of nuclear data uncertainties on reactivity changes of SNEAK-12B core. Prog. Nucl. Energy 105, 124–135.

Rohatgi, A., 2018. WebPlotDigitizer, version 4.1. <https://automeris.io/WebPlotDigitizer>.

Ruggieri, J.M., Tommasi, J., Lebart, J.F., Suteau, C., Plisson-Rieunier, D., De Saint Jean, C., Rimpault, G., Sublet, J.C., 1973. ERANOS 2.1: international code system for GEN-IV fast reactor analysis. In: Proc. ICAAP2006. American Nuclear Society, Reno, NV, USA.

Santamarina, A., Bernard, D., Blaise, P., Coste, M., Courcelle, A., Huynh, T.D., Jouanne, C., Leconte, P., Litaize, O., Mengelle, S., Noguere, G., Reggieri, J.-M., Serot, O., Tommasi, J., Vaglio, C., Vidal, J.-F., 2009. The JEFF-3.1.1 Nuclear Data Library, Tech. Rep. JEFF Report 22. OECD/NEA Data Bank.

Sartori, E., 1990. Standard Energy Group Structure of Cross Section Libraries for Reactor Shielding, Reactor Cell and Fusion Neutronic Applications: VITAMIN-J, ECCO-33, ECCO-2000 and XMAS, Tech. Rep. JEF/DOC-315 Revision 3 – DRAFT. OECD/NEA Data Bank.

Tommasi, J., Archier, P., Rimpault, G., 2010. Sodium void validation with ERANOS on zero power facility experiments. In: Proc. PHYSOR-2010. American Nuclear Society, Pittsburgh, PA, USA.

X-5 Monte Carlo Team, 2003. MCNP – Version 5, Vol. I: Overview and Theory, LA-UR-03-1987.